

Y. Tsujimoto

Osaka University,
Faculty of Engineering Science,
1-1 Machikaneyama,
Toyonaka, Osaka, 560 Japan

A. J. Acosta

C. E. Brennen

California Institute of Technology,
Division of Engineering
and Applied Science,
Pasadena, CA 91125

Theoretical Study of Fluid Forces on a Centrifugal Impeller Rotating and Whirling in a Volute

Fluid forces on a rotating and whirling centrifugal impeller in a volute are analyzed with the assumption of a two-dimensional rotational, inviscid flow. For simplicity, the flow is assumed to be perfectly guided by the impeller vanes. The theory predicts the tangential and the radial force on the whirling impeller as functions of impeller geometry, volute spacing, and whirl ratio. A good qualitative agreement with experiment is found.

1 Introduction

Along with the developments of high-speed and high-performance turbomachines, there has been increasing occurrence of rotational speeds higher than the first critical speed. Under these circumstances, turbomachines may suffer from severe vibration and rotor whirl caused by fluid-dynamic forces. As possible causes of whirling instabilities, fluid forces on journal bearings and seals are well known and extensive studies have been made of these effects. Recently, experiments have shown that the fluid forces on the impeller itself can be a cause of the whirl instabilities. Ohashi and Shoji (1984) measured unsteady fluid forces on two-dimensional centrifugal impellers whirling in a vaneless diffuser, for various whirl ratios and flow coefficients. Their purpose was to obtain fundamental data for rotor whirl and to compare the results with their theoretical estimates of the effect. They found that, in most cases, the fluid forces have a damping effect on the whirling motion but they observed destabilizing fluid forces for forward whirling motion at lower flow coefficients near shut off and in a range of small whirl speed ratio. At nearly the same time, experiments on three-dimensional impellers with a volute were made at Caltech for direct use in design. Fluid forces were measured quasistatically (Chamieh et al., 1982) and dynamically (Jery et al., 1984). In the first of these it was shown that the quasisteady fluid forces have a destabilizing effect for forward whirl and in the second that the region of instability is similar to that observed by Ohashi and Shoji (1984). The major differences from Ohashi and Shoji's results were that: (i) measured forces are much larger, and (ii) destabilizing forces are also observed near the design flow coefficient. More recently, experimental results on a strictly two-dimensional radial impeller in the same volute have become available (Arndt and Franz, 1986). The magnitudes of the impeller forces are significantly reduced but the contrast with Ohashi and Shoji's results without volutes still remain. It has been shown (Adkins, 1986) that the large difference between the forces on the 3-D and 2-D impellers in the volute is

due to the distribution of pressure on the external surface of the shroud of the 3-D impeller.

All of the above measurements were carried out by using circular whirling orbits. Bolleter et al. (1987) used a "rocking arm" test apparatus to measure force matrices of boiler feed pump impellers with outlet guide vanes. Much larger destabilizing whirling forces than those found at Caltech were measured near the best efficiency point and in a range of positive whirl speed ratio, possibly because of the small radial clearance between the impeller and the vaned diffuser or small front shroud/housing clearance.

Most of the early theoretical models (Thompson, 1978, Colding-Jorgensen, 1980, Chamieh and Acosta, 1981) were based on the assumption of quasi-steady flow which restricts their application to the case of very small whirl speed. Recently Adkins (1986) and Adkins and Brennen (1988) presented a dynamic analysis which includes the unsteadiness in both the impeller and the volute flows. Flows in both components were treated one-dimensionally and both forces and hydrodynamic force matrices were compared with experimental results for whirl speed/shaft speed ratios up to 0.2. The one-dimensional theory yielded forces in good agreement with the experiments and hydrodynamic matrices which exhibited the correct qualitative characteristics.

The present paper is similar to those of Shoji and Ohashi in that it examines the two or three-dimensional character of the unsteady flow in order to establish the complex relationship between the vorticity shed by the impeller blades and the forces on the impeller. Shoji and Ohashi (1980, 1984) performed unsteady flow analyses by singularity methods. Their model is complete in the sense that the effects of shed vorticity are fully taken into account and impellers with a finite number of vanes are treated under the assumption of two-dimensional, inviscid, incompressible and nonseparated flow. The computations are compared with experiment in Ohashi and Shoji (1984). Near the design flow rate their model can predict fluid forces quite accurately. But the destabilizing fluid force at lower flow coefficient observed in their experiments cannot be simulated by the potential flow calculations. They also made calculations (Shoji and Ohashi, 1984) with diffuser vanes in

Contributed by the Technical Committee on Vibration and Sound for publication in the JOURNAL OF VIBRATION, ACOUSTICS, STRESS, AND RELIABILITY IN DESIGN. Manuscript received July 30, 1986.

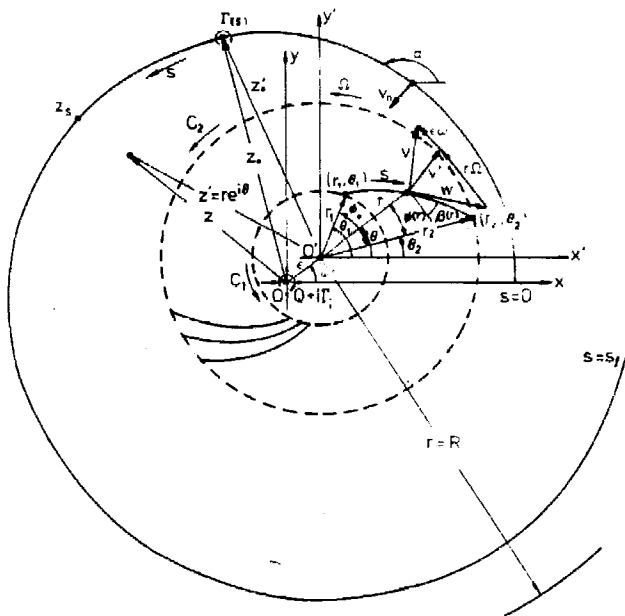


Fig. 1 Impeller and volute configuration. The volute is represented by the solid spiral; the impeller is indicated by the dotted lines with a few representative vanes sketched in. The center of the impeller is at O' and it is displaced a distance ϵ from the volute center O .

which only the effects of a steady vortex distribution on the vanes were taken into account.

The present study analyzes the fluid forces on a two-dimensional centrifugal impeller rotating and whirling in a volute, with special emphasis on unsteady interaction effects. As an extension of Chamieh and Acosta (1981), it is assumed that the number of the impeller vanes is so large that the flow in the impeller is perfectly guided by the vanes, so that the impeller is replaced by an "actuator disk." Because of this assumption only qualitative agreements are expected when applied to realistic impellers. But the present analysis has the following advantages. For impellers with a finite number of vanes, superposition of the unsteadiness due to the passage of each vane on the unsteadiness due to the whirling motion

becomes very complicated. The actuator assumption removes the former unsteadiness and the flow model becomes greatly simplified. In addition, this approach makes it possible to have an empirical total pressure loss in the impeller.

In principle, the present problem can be treated in the same way as Shoji and Ohashi (1984) in their impeller/guide vane interaction problem. We simplify the problem by applying the actuator disk assumption but also take into account the effects of the unsteady vortex distributions on the volute.

Thus the following assumptions are made in the present study:

- (1) The flow is two dimensional, inviscid and incompressible.
- (2) The flow in the impeller flow passage is perfectly guided by the vanes.
- (3) The impeller executes a whirling motion with a small and constant eccentricity ϵ and with a constant whirling angular velocity ω . Hence, quantities of order ϵ^2 are neglected.
- (4) Vorticity is transported on a prescribed mean flow.
- (5) The volute can be simulated by a curved plate.

2 Basic Equations

We consider an impeller with large number of vanes executing a whirling motion in a volute casing as shown in Fig. 1. It is convenient here to work in a rotating and translating frame fixed to the rotor. Euler's equation in this frame can be expressed (for the derivation of equations (1) and (2), see the Appendix);

$$\frac{\partial \mathbf{v}}{\partial t^*} + \nabla H' - \mathbf{w} \times (\nabla \times \mathbf{v}) = \mathbf{f} \quad (1)$$

where

$$H' = \frac{1}{2} \mathbf{w}^2 - \frac{1}{2} (\mathbf{U} + \boldsymbol{\Omega} \times \mathbf{x}')^2 + \frac{p}{\rho}$$

and $\partial/\partial t^* = \partial/\partial t + \boldsymbol{\Omega} \partial/\partial \theta$ is the time derivative in the rotating frame. $\mathbf{U} = i\omega \epsilon e^{i\omega t}$ and $\boldsymbol{\Omega} \times \mathbf{x}' = i\boldsymbol{\Omega} e^{i\theta}$ are the translational velocity due to whirling and the rotational velocity of the impeller. We now integrate the component of equation (1) parallel to the vane surface from inlet to outlet along a vane surface to obtain the following expression for the total pressure increase in the impeller

Nomenclature

$[A_{ij}]$	= hydrodynamic force matrix
\mathbf{f}	= external force exerted by impeller vanes
F_x^*, F_y^*	= normalized lateral force in x and y direction
F_n, F_t	= time average of normal and tangential components of normalized unsteady force
i	= imaginary unit
p, p_t	= pressure, total pressure, $p_t \equiv p + (\rho/2)v^2$
r_1, r_2	= inner and outer radius of impeller
Q	= flow rate
R	= radius of a circle, vorticity within which is considered
t	= time
$\mathbf{v} = \mathbf{u} - i\mathbf{v}$	= $\mathbf{u}' - i\mathbf{v}' - i\omega \epsilon e^{-i\omega t}$; absolute velocity
$\mathbf{v}' = \mathbf{u}' - i\mathbf{v}'$	= $(v_r' - iv_\theta')e^{-i\theta}$; velocity relative to z' frame
\mathbf{w}	= velocity relative to impeller
$z = x + iy$	= stationary frame with its origin O fixed to the center of the whirling motion
$z' = x' + iy'$	= $re^{i\theta} = z - \epsilon e^{i\omega t}$; translating frame with its origin O' fixed to the center of impeller and its axes parallel to those of z

β	= vane angle
Γ_i	= circulation of prerotation
$\Gamma, \Gamma_s, \Gamma_d^s, \Gamma_d^c$	= vortex distribution on volute, its steady component; unsteady components with sine and cosine time dependence
$\epsilon (\ll r_2)$	= eccentricity
ϵ_x, ϵ_y	= dislocations in x and y direction
ζ	= vorticity
ρ	= density
$\varphi = Q/2\pi r_2^2 \Omega$	= flow coefficient
ω	= angular velocity of whirling motion
Ω	= angular velocity of impeller
ω/Ω	= whirl speed ratio

Subscripts

- 1, 2 = quantities at the inner and outer radius of impeller
 n, t = components normal to and tangential to the whirling orbit (positive outwards and counterclockwise)

$$\frac{p_{i2} - p_{i1}}{\rho} = [r\Omega v_{\theta'}]_1^2 - M \left(\frac{\partial}{\partial t} + \Omega \frac{\partial}{\partial \theta} \right) v'_{z_2} - \epsilon \omega (\Omega - \omega) \int_1^2 \sin(\theta + \beta - \omega t) ds + \epsilon \omega [(r\Omega + v_z) \cos(\theta - \omega t) + v'_r \sin(\theta - \omega t)]_1^2 \quad (2)$$

where

$$M = \int_1^2 \frac{r_2 ds}{r \sin \beta}, \quad [f(x)]_1^2 = f(x_2) - f(x_1)$$

We have assumed that the external force f exerted by impeller vanes is normal to the vane surface.

Outside of the impeller, where $f = 0$, the θ -component of equation (1) can be represented by

$$\zeta = \frac{\partial v}{\partial x} - \frac{\partial u}{\partial y} = \frac{1}{v'_r} \left(\frac{\partial v_{\theta'}}{\partial t^*} + \frac{\partial H'}{r \partial \theta} \right) \quad (3)$$

The vorticity at the outlet of the impeller can be obtained by applying equation (3) at $r = r_2$. In this equation H'_2 is determined as follows. $H'_2 - H'_1$ is obtained through the integration of the component of equation (1) parallel to the vane surface. We assume that the flow is irrotational upstream of the impeller. Hence, we can use equation (3) with $\zeta = 0$ at $r = r_1$. This gives a relation for H'_1 , which is used in equation (3) at $r = r_2$ along with the $H'_2 - H'_1$ obtained above. By this procedure we arrive at the following expression

$$\zeta(r_2, \theta) = -\frac{1}{r_2 v'_r} \left[\frac{\partial}{\partial t^*} (r_2 v_{\theta 2} - r_1 v_{\theta 1}) - M \frac{\partial^2 v'_{z_2}}{\partial t^* \partial \theta} - \epsilon \omega (\Omega - \omega) \int_1^2 \cos(\theta + \beta - \omega t) ds \right] \quad (4)$$

The first term represents the effect of the change in Euler head; the second and the third terms represent the effects of the changes in the inertia due to acceleration in relative flow and to whirling motion, respectively.

3 Elementary Flow Components

Since we linearize the problem, the flow in the volute can be represented by a sum of elementary flow components. In this section we prepare flow components satisfying the boundary condition at the impeller outlet to be used for the construction of the entire flow field.

The flow tangency condition at the impeller outlet is;

$$v'_{\theta 2} = r_2 \Omega - v'_{r 2} \cot \beta_2 \quad (5)$$

The first term on the right-hand side of the above equation is cancelled by the steady flow component

$$u' - iv' = \frac{1}{2\pi z'} \left(Q - 2\pi i r_2 \left(r_2 \Omega - \frac{Q}{2\pi r_2} \cot \beta_2 \right) \right) \quad (6)$$

and other disturbance components should satisfy the following equation

$$v'_{\theta 2} = -v'_{r 2} \cot \beta_2 \quad (7)$$

In the region outside the impeller, we consider the following three types of elementary flow components satisfying equation (7):

3.1 Velocity Induced by the Vortex Distribution on the Volute. In order to represent the effect of volute, we consider the following velocity field.

$$u' - iv' = \frac{i\Gamma(s) ds}{2\pi} \left\{ \frac{1}{z' - z'_0} + e^{-2i\beta_2} \left(\frac{1}{z'} - \frac{1}{z' - r_2^2/z'_0} \right) \right\} \quad (8)$$

The first term represents a vortex of strength $\Gamma(s) ds$ at $z' = z'_0(s)$. The second term represents a flow due to a source-

vortex at the mirror image of z'_0 with respect to the circle $r = r_2$, and one at the origin. This term is added so that the total flow satisfies the boundary condition (7). This expression shows that the flow component has no circulation around the impeller and no flow rate from the impeller. The effect of the volute is represented by a super-position of this flow component, i.e., by the integral of equation (8) along the volute. We consider steady ($\Gamma_s(s)$) and unsteady ($(\epsilon/r_2)\Gamma_d^s(s)$, $(\epsilon/r_2)\Gamma_d^c(s)$) vortex components and put

$$\Gamma(s) = \Gamma_s(s) + (\epsilon/r_2)\Gamma_d^s(s) \sin \omega t + (\epsilon/r_2)\Gamma_d^c(s) \cos \omega t$$

in equation (8).

3.2 Velocity Induced by Shed Vorticity. As shown in the last section, the vorticity is shed from the impeller due to the unsteadiness of the flow relative to the impeller. We assume that the velocity is transported on the log-spiral flow

$$u' - iv' = \frac{Q_s - i\Gamma_s}{2\pi z'} \quad (9)$$

Then we have the following elementary vorticity field

$$\zeta_n = \zeta_{cn} \cos \Phi + \zeta_{sn} \sin \Phi$$

$$\Phi = \pm \omega \left\{ t - \frac{\pi}{Q_s} (r^2 - r_2^2) \right\} + n \left\{ \theta - \frac{\Gamma_s}{Q_s} \log \left(\frac{r}{r_2} \right) \right\} \quad (10)$$

The velocity induced by this vorticity field is

$$v'_{rn} - iv'_{\theta n} = (\zeta_{cn} Z_{Rn} + \zeta_{sn} Z_{In}) \cos(n\theta \pm \omega t) + (\zeta_{sn} Z_{Rn} - \zeta_{cn} Z_{In}) \sin(n\theta \pm \omega t) \quad (11)$$

where

$$Z_{Rn} = R_{Rn} - i\theta_{Rn}, \quad Z_{In} = R_{In} - i\theta_{In},$$

$$R_{Rn} = \text{Real}[i\{F(r) + G(r)\}], \quad R_{In} = \text{Imag}[i\{F(r) + G(r)\}]$$

$$\theta_{Rn} = \text{Real}[i\{F(r) - G(r)\}], \quad \theta_{In} = \text{Imag}[i\{F(r) - G(r)\}]$$

$$\left. \begin{aligned} F(r) &= \frac{1}{2} \int_{r_2}^r e^{i\Phi'} (r_0/r)^{n+1} dr_0 \\ G(r) &= \frac{1}{2} \int_r^R e^{i\Phi'} (r/r_0)^{n-1} dr_0 \end{aligned} \right\}$$

$$\Phi' = \mp \frac{\pi\omega}{Q_s} (r_0^2 - r_2^2) - n \frac{\Gamma_s}{Q_s} \log(r_0/r_2) \quad (11')$$

Expression (11) is obtained by integrating the velocity induced by ζ_n of equation (10) in $r_2 < r < R$. We add a potential flow component

$$v'_{rn} - iv'_{\theta n} = -e^{-i\beta_2} (\zeta_{cn} + i\zeta_{sn}) \times [(\theta_{Rn} - i\theta_{In}) \sin \beta_2 + (R_{Rn} - iR_{In}) \cos \beta_2]_{r=r_2} \frac{e^{i\theta \mp \omega t}}{z'^{n+1}}, \quad (12)$$

so that the total flow

$$v'_r - iv'_{\theta} = (v'_{rn} - iv'_{\theta n}) + (v'_{rn} - iv'_{\theta n}) \quad (13)$$

satisfies the boundary condition of equation (7) and represents the effect of shed vorticity.

3.3 Conditions at Infinity. There we require the absolute velocity to vanish at $z' = \infty$. In order to cancel the velocity due to whirl at infinity, put

$$u' - iv' = i\omega \epsilon [e^{-i\omega t} + \left(\frac{r_2}{z'} \right)^2 e^{i(\omega t - 2\beta_2)}] \quad (14)$$

The first term cancels the whirl velocity and the potential flow of the second term is added so that the boundary condition (7) remains satisfied.

We may now note that the flow downstream of the impeller

can be represented by a sum of the elementary flow components represented by equations (6), (8), (13), and (14). The total flow satisfies the conditions at infinity and at the exit of the impeller.

3.4 Flow in the Upstream Region. In the region upstream of the impeller ($r < r_1$), the flow can be assumed to be irrotational. We put a source Q and a vortex Γ_i at the center of whirl to represent the effects of flow rate and prerotation. Then the flow can be represented by

$$u' - iv' = \frac{Q + i\Gamma_i}{2\pi} \frac{1}{z' + \epsilon e^{i\omega t}} + \sum_{n=1}^{\infty} \{ \bar{A}_n + \epsilon (A_n^s \sin \omega t + A_n^c \cos \omega t) \} z'^{n-1} \quad (15)$$

where \bar{A}_n , A_n^c and A_n^s are unknown complex constants.

4 Method of Solution

In the preceding section we have given all of the elementary flow components required for the construction of the entire flow field. These components satisfy the conditions upstream and downstream of the impeller and the flow tangency condition at the outlet of the impeller. But they contain several unknowns to be determined by using the following conditions:

4.1 Continuity Equation. Since the flow in the impeller is perfectly guided by the vanes, the continuity equation can be represented as follows.

$$r_1 v_{r1}'(r_1, \theta_1) = r_2 v_{r2}'(r_2, \theta_2) \quad (16)$$

where $\theta_1 = \theta_2 + \phi_0$ and θ_2 are angular positions of a vane surface at $r = r_1$ and at $r = r_2$, respectively. This equation determines the unknown constants representing the flow upstream of the impeller.

4.2 Strength of Shed Vorticity. The strength of shed vorticity at the outlet of the impeller is determined by equation (4). Since the fundamental vorticity distribution in equation (10) is represented in a form of a Fourier component with respect to θ , it is convenient to represent the velocities at the inlet and outlet of the impeller in Fourier Series. Then equation (4), and equation (16) give relations governing these Fourier coefficients.

4.3 Boundary Condition on the Volute Surface. The condition that the normal component of the absolute velocity should vanish on the volute, i.e., the flow tangency condition, is

$$\epsilon \omega \cos(\omega t - \alpha) + v_r' \sin(\theta - \alpha) + v_\theta' \cos(\theta - \alpha) = 0 \quad (17)$$

where α is the angle between the volute and x -axis. The velocities (v_r' , v_θ') on the volute surface $z = z_s$, are obtained by putting $z' = z_s - \epsilon e^{i\omega t}$ in equations (6), (8), (13), and (14) and linearizing them on the assumption that $\epsilon < r_2$. Then equation (17) gives an integral equation with respect to the vortex distribution $\Gamma(s)$ on the volute. This equation can be reduced to $N-1$ linear simultaneous equations if we specify the strength of the vortex distribution at N discrete position (vortex points) on the volute as unknowns and apply equation (17) at $N-1$ points between the vortex points. Further, we should use an unsteady Kutta condition (Tsujimoto et al., 1986)

$$\frac{d}{dt} \int_0^{s_1} \Gamma(s) ds = -\Gamma(s_1) w(s_1) \quad (18)$$

where $w(s_1)$ is the average of the velocities on the upper and lower surface of the volute trailing edge. This equation states that the amount of the change of the circulation on the volute is shed from the trailing edge as a free vortex distribution with

strength $\Gamma(s_1)$. If we strictly adhere to the present two-dimensional model, we should take account of the effect of the shed free vortex distribution. Considering that we are modelling a three-dimensional volute which is connected to an outlet pipe, it is unrealistic to expect that the free vortex distribution would play an important role in the determination of the fluid forces on the impeller. For this reason and for simplicity, we neglect the effects of free vortex distribution shed from the volute, while using equation (18) as a supplementary condition to equation (17). Now we have N linear equations to determine the strength of the vortex distribution on N vortex points.

The conditions stated in this section, i.e., equations (4), (16), (17), and (18) give a complete set of linear simultaneous equations to determine the unknown constants included in the expressions of elementary flow components. The flow components and the above relations can be divided into steady parts of order ϵ^0 and unsteady parts of ϵ^1 after linearization with respect to $\epsilon < r_2$. The steady parts can be solved independently of the unsteady parts and the latter parts are solved by using the results for steady parts.

5 Fluid Forces on the Impeller

By considering the balance of the momentum of the fluid in the impeller, we can express the forces on the impeller as follows.

$$\begin{aligned} F_{x'} - iF_{y'} = & -i \left(\oint_{c_2} - \oint_{c_1} \right) p_{\Omega} dz' \\ & + \frac{i\rho}{2} \left(\oint_{c_2} - \oint_{c_1} \right) (u' - iv')^2 dz' \\ & + i\rho\omega \epsilon \left(\oint_{c_2} - \oint_{c_1} \right) (u' - iv') \cos(\theta - \omega t) r d\theta \\ & - \rho \frac{d}{dt} \int_S \int_S v_r'(r_2, \theta_2 = \theta - \phi(r)) \\ & \times \frac{r_2}{r \sin \beta} e^{-i(\theta - \pi/2 + \beta)} r dr d\theta \\ & + \rho\omega^2 \epsilon \pi (r_2^2 - r_1^2) e^{-i\omega t} \end{aligned} \quad (19)$$

where c_1 and c_2 represent counterclockwise integrals on $r = r_1$ and r_2 , respectively, and S means an integral over a region surrounded by the circles with $r = r_1$ and r_2 . The azimuthal angle $\theta_2 = \theta - \phi(r)$ gives the angular position at $r = r_2$ of the vane which passes through the point (r, θ) .

For the integration of the total pressure on $r = r_1$, we should make use of equation (3) with $\zeta = 0$, and equation (2) is used for the integration on $r = r_2$. Then each term in the right-hand side of equation (19) is represented as integrals of the velocities on $r = r_1$ and r_2 , that can be easily evaluated if we use the Fourier representation of the velocities. Equation (19) is used after linearization and separation into steady and unsteady components.

6 Results and Discussion

In order to assess the present model, calculations were made on an impeller and a volute simulating those used in the experiments by Chamieh et al. (1982) and Jery et al. (1984) carried out at Caltech. The "Impeller X" used in the experiments is modelled by a two-dimensional logarithmic spiral with $\beta = 25$ deg and $r_1/r_2 = 0.4$. The "Volute A" is modelled by logarithmic vane represented by

$$r = 1.123 e^{\theta \times \tan 6.538^\circ}, 0 \text{ deg} < \theta < 396 \text{ deg.}$$

The volute angle is determined so that the volute surface coincides with a streamline of a flow due to flow rate Q and it

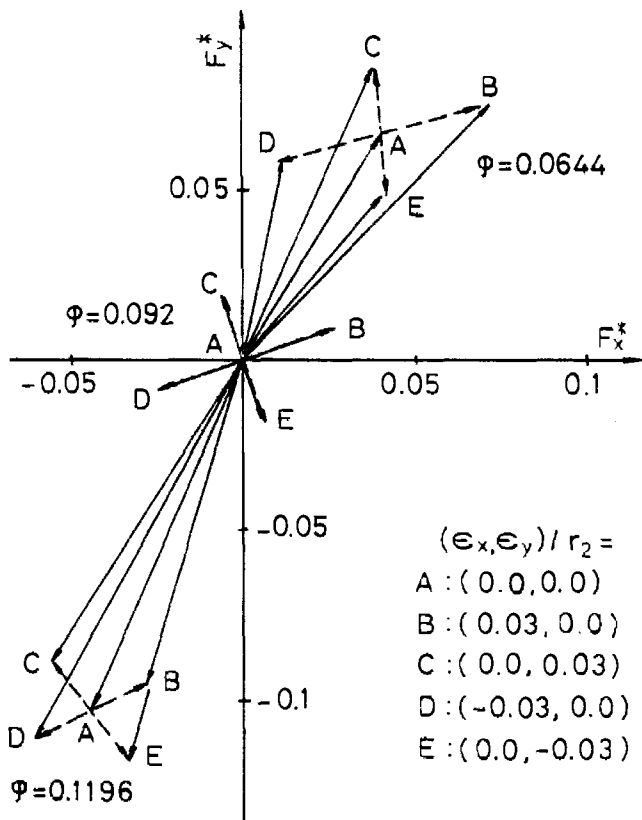


Fig. 2 Calculated lateral forces F_x^* , F_y^* for the impeller X/Volute A combination for various displacements ϵ_x , ϵ_y of the impeller center.

impeller circulation at design flow coefficient ($\phi = 0.092$) of the experiments. The radial position of the tongue ($r_1/r_2 = 1.123$) is set to be the same as "Volute A."

Calculations of the steady component are carried out first and the steady vortex distribution $\Gamma_s(s)$ thus obtained is used in the calculation of the unsteady components. Since the integrals in equation (11) involving the velocities induced by shed vorticity do not converge in the limit $R \rightarrow \infty$ for the cases of $\omega = 0$ and $n < 2$, it was assumed that the vorticity in the volute decayed like $1/r^2$. Thus we used $R/r_2 = 5.0$ for all of the vorticity components. This might be justified if we argue that the vorticity outside the volute should have little effect on the forces on the impeller and that the shed vorticity will decay due to mixing in the volute.

Furthermore, since the flow in the volute is nearly perfectly guided we use a value of Γ_r in equation (9) such that the velocity with $Q_r = Q$ is tangential to the volute surface. For the calculations without a volute, the flow rate Q was used with the corresponding impeller circulation for Q_r and Γ_r . Only cases with zero prerotation were evaluated ($\Gamma_i = 0$).

The vortex distribution is discretized to N vortex points given by

$$\theta_n = 198 \text{ deg} \times [1 - \cos\{\pi(n-1)/(N-1)\}], n = 1 \dots N$$

and finite Fourier representations with M terms are used for the velocities at $r = r_1$ and r_2 . To conserve computational time, values of $M = 5$ and $N = 30$ were employed, since the calculated values of lateral forces did not change by more than 3 percent when the values of M or N were doubled.

Figure 2 shows lateral forces on the impeller in which the center of the impeller is moved to $(x, y) = (\epsilon_x, \epsilon_y)$. Lateral forces (F_x, F_y) per unit impeller outlet width are normalized as follows

$$(F_x^*, F_y^*) = (F_x, F_y) / \rho \pi (r_2 \Omega)^2 r_2.$$

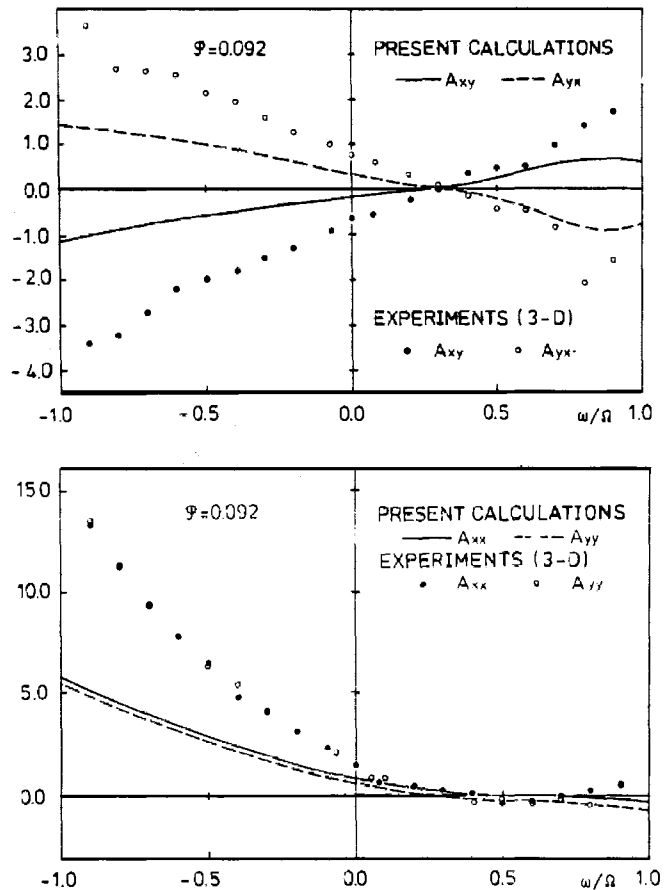


Fig. 3 The hydrodynamic force matrix components for Impeller X/Volute A. Measured values are from Jery et al. (1984). Note the qualitative similarity between the present calculations and the experiments.

Solid arrows in the figure indicate the results obtained by actually moving the impeller in the computer program for the analysis of steady component and the dotted ones are obtained by putting $\omega = 0$ in the unsteady program. The small discrepancies are believed to be due to the linearization used in the analysis of unsteady component. This figure shows the validity of the linearization for eccentricities of this order.

We see that the force vector due to the displacement (dotted arrows) are rotated counterclockwise by about 20 deg from the direction of the displacement. This shows that the quasisteady fluid forces have a destabilizing character for whirl in the direction of the rotation of the rotor. This is in accord with the quasisteady measurements of Chamieh et al., 1982.

Unsteady force components (\bar{F}_x, \bar{F}_y) on the impeller per unit impeller outlet width are represented by

$$\begin{pmatrix} \bar{F}_x \\ \bar{F}_y \end{pmatrix} = \rho \pi (r_2 \Omega)^2 \begin{bmatrix} A_{xx} & A_{xy} \\ A_{yx} & A_{yy} \end{bmatrix} \begin{pmatrix} \epsilon \cos \omega t \\ \epsilon \sin \omega t \end{pmatrix}$$

where $[A_{ij}]$ is called the hydrodynamic force matrix. Figure 3 includes the experimental results of Jery et al., 1984 and calculated values of A_{ij} for Impeller X/Volute A as function of the whirl speed ratio ω/Ω from the present theory. Although the present model like that of Adkins and Brennen (1988) underestimates the force matrix elements we do observe a qualitative agreement. In cases without a volute, we find that $A_{xx} = A_{yy}$ and $A_{xy} = -A_{yx}$ because of the symmetry of the flow. Deviations from this symmetry are caused by the effect of the volute. The unsteady force may be decomposed into components normal to and tangential to the whirling orbit. These components are constant around the orbit if there is no volute. But if there is a volute there are variations around the

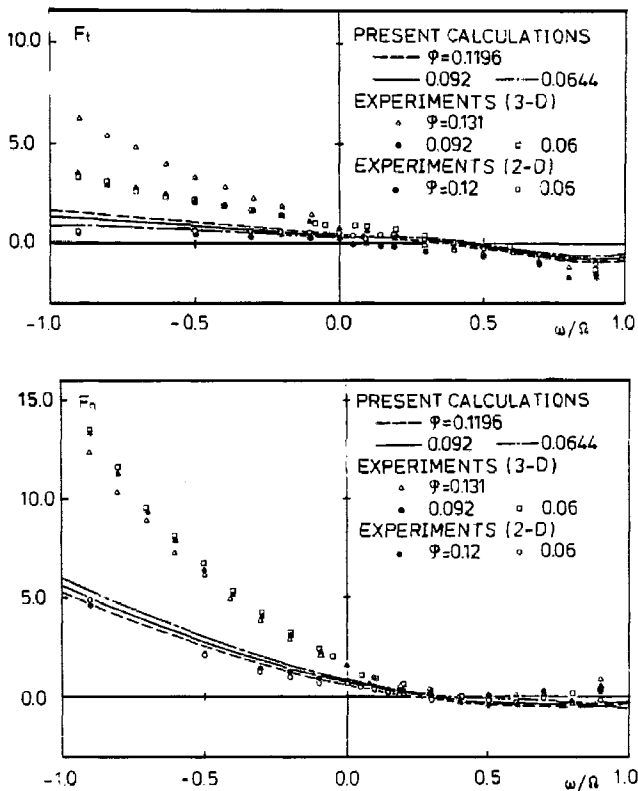


Fig. 4 The tangential and normal force $F_t = 1/2(A_{yx} - A_{xy})$, $F_n = 1/2(A_{xx} + A_{yy})$ for Impeller X/Volute A. Calculated values are compared with two and three-dimensional impeller measurements (2-D, 3-D) of Arndt and Franz (1986) and Jery et al. (1984).

orbit but the average value of the tangential component over an orbit has a special meaning in rotordynamics; if the average tangential force is in the direction of the whirling motion, this force promotes the whirling motion. In other words, the fluid forces are rotordynamically destabilizing. The time averages or average around the orbit of the normal and tangential components (F_n , F_t) normalized by $\rho\pi(r_2\Omega)^2\epsilon$ are given by

$$\begin{pmatrix} F_n \\ F_t \end{pmatrix} = \frac{1}{2} \begin{pmatrix} A_{xx} + A_{yy} \\ A_{yx} - A_{xy} \end{pmatrix}$$

Figure 4 shows experimental (Jery et al., 1984) and calculated values of the normal and tangential forces on Impeller X/Volute A. We note that experimental values of F_t is positive in the region $0 < \omega/\Omega < 0.4$, which shows that the fluid forces are destabilizing in that interval. This destabilizing effect emerges from the present theory. The effects of flow coefficient and whirl speed ratio are also well simulated.

More recently, experimental results on a strictly two-dimensional, radial impeller with flat radial shrouds have been made available by Arndt and Franz (1986). The hydraulic performance of this impeller is very similar to that of Impeller X. The tangential and normal forces of this impeller measured in Volute A are shown in Fig. 4. The agreement with the present theory is, we believe, quite satisfactory. The large difference between these experimental results and those of Jery et al. (1984) have been shown by Adkins (1986) and Adkins and Brennen (1988) to be due to the distribution of pressure on the external surface of the shroud of Impeller X.

Figure 5 shows the calculated results for Impeller X without a volute. The forces are much smaller than those in Fig. 4. No destabilizing region is now observed and the values of F_n and F_t at $\omega/\Omega = 0$ are very small. In the experiments on two-dimensional impeller/vaneless diffusers, Ohashi and Shoji (1984) measured much smaller fluid forces than those in Fig. 4

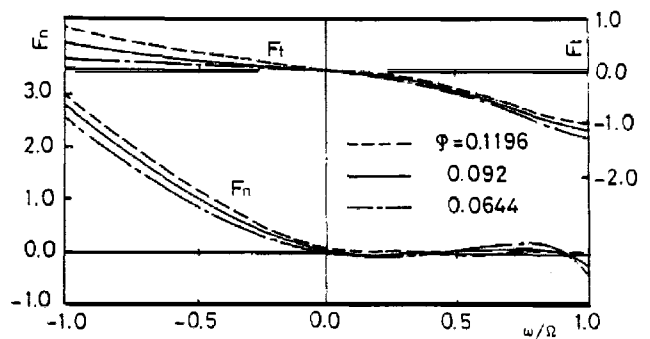


Fig. 5 The tangential and normal forces on Impeller X, without volute.

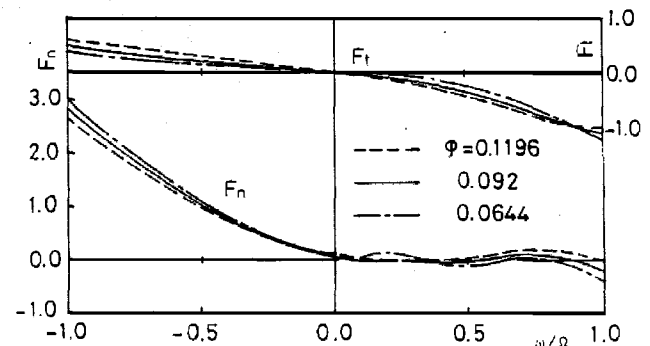


Fig. 6 The tangential and normal forces on Impeller X/Volute A, when the effects of unsteady vortex distributions on the volute are neglected.

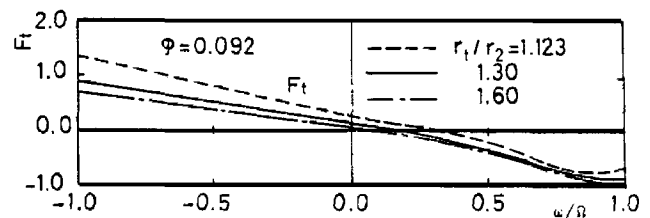


Fig. 7 Effects of the radial position r_1/r_2 of the tongue on the tangential force F_t .

and did not find any destabilizing forces near design flow rate. They also measured very small forces at $\omega/\Omega = 0$. Our results in Fig. 5 exhibit similar features and imply that the unsteady interaction effects of the whirling impeller with the volute can be a cause of the difference between the experimental results shown in Fig. 4 and those by Ohashi and Shoji (1984).

It has been shown by Chamieh and Acosta (1979) and also independently by Ohashi and Shoji (1984) that the normal force F_n is approximated by a sum of the centrifugal force on the apparent mass of the impeller and the Joukowski force on the impeller circulation. The normal force in Fig. 5 can be approximated by the centrifugal force and the Joukowski force by using the apparent mass given by Chamieh and Acosta (1979).

In the calculations of the interaction effects between adjacent blade rows in axial flow machines, it is often assumed that the unsteady vortex distribution on the opposite blade row can be neglected. Figure 6 shows the results for Impeller X/Volute A obtained by putting $\Gamma_d^s = \Gamma_d^v = 0$. We see that this result fails to reproduce the important effects of unsteady interaction as observed in Fig. 4. It shows that we cannot neglect the effects of unsteady vortex distributions on the volute in treating the whirl/volute interaction problem in which the influence on the flow by the volute is very large.

Figure 7 shows the effect of radial position r_1/r_2 of the

tongue on F_t . The volute angle is kept constant. The region of destabilization does diminish as r_1/r_2 is increased but it requires the use of a vaneless diffuser with inner to outer radius ratio larger than 1.6 to substantially remove the region. This implies that the destabilization is not caused by a local interaction with tongue but by an interaction with the volute as a whole.

7 Conclusion

An inviscid linearized, rotational flow model of the interaction between a whirling, eccentric two-dimensional impeller and surrounding volute is presented. Force matrices due to the displacement of the eccentric impeller are calculated as a function of whirl-impeller speed ratio for a range of flow rates and impeller-volute geometry. The force matrix is shown to be nearly skew-symmetric and, depending on the volute clearance, to have a region of destabilizing tangential force. The results of these computations are shown to agree well with experimental measurements on a two-dimensional test impeller.

8 Acknowledgments

The authors are grateful for the support by the National Aeronautics and Space Administration under Contract NAS8-33108. One of the authors (Y.T.) would like to thank also Yamada Science Foundation for their financial support for his stay at Caltech. His acknowledgments are also to Professor K. Imaichi and Dr. O. Furuya for their continued encouragement, to Mr. M. Hirao for his support in numerical calculations, and to the people in Caltech for their warm hospitality and friendships.

References

Adkins, D., 1986, "Analysis of Hydrodynamic Forces on Centrifugal Impellers," California Institute of Technology, Ph.D. thesis.
 Adkins, D. R., Brennen, C. E., 1988, "Analyses of Hydrodynamic Radial Forces in Centrifugal Pump Impellers," *ASME Journal of Fluids Engineering*, Vol. 110, No. 1, pp. 20-28.
 Arndt, N., and Franz, R., 1986, "Measurements of Hydrodynamic Forces on a Two-Dimensional Impeller and a Modified Centrifugal Pump," Division of Engineering and Applied Science, California Institute of Technology, Rept. E249.4.
 Bolleter, U., Wyss, A., Welte, I., and Stürchler, R., 1987, "Measurement of Hydrodynamic Interaction Matrices of Boiler Feed Pump Impellers," *ASME JOURNAL OF VIBRATION, ACOUSTICS, STRESS, AND RELIABILITY IN DESIGN*, Vol. 109, No. 2, pp. 144-151.
 Chamieh, D. S., and Acosta, A. J., 1979, "Dynamic Forces on a Whirling Centrifugal Rotor," Proc. 13th Conf. on Fluid Machinery, Akademiai Kiado, Budapest, Hungary.
 Chamieh, D. S., and Acosta, A. J., 1981, "Calculation of the Stiffness Matrix of an Impeller Eccentrically located within a Volute," Cavitation and Polyphase Flow Forum, Joint ASME/ASCE Conf., Boulder, Colorado, pp. 51-53.
 Chamieh, D. S., Acosta, A. J., Brennen, C. E., Caughey, T. K., and Franz, R., 1982, "Experimental Measurements of Hydrodynamic Stiffness Matrices for a Centrifugal Pump Impeller," NASA CP 2250, pp. 382-398.
 Colding-Jorgensen, J., 1980, "Effect of Fluid Forces on Rotor Stability of Centrifugal Compressors and Pumps," NASA CP 2133, pp. 249-265.
 Jery, B., Acosta, A. J., Brennen, C. E., and Caughey, T. K., 1984, "Hydrodynamic Impeller Stiffness, Damping, and Inertia in the Rotordynamics of Centrifugal Flow Pumps," NASA CP 2335, pp. 137-160.
 Milne-Thomson, L. M., 1968, "Theoretical Hydrodynamics," 5th ed., Macmillan and Co. Ltd., London.
 Ohashi, H., and Shoji, H., 1984, "Lateral Fluid Forces Acting on a Whirling Centrifugal Impeller," NASA CP 2335, pp. 109-122.
 Shoji, H., and Ohashi, H., 1980, "Fluid Forces on Rotating Centrifugal Impeller with Whirling Motion," NASA CP 2133, pp. 317-328.
 Shoji, H., and Ohashi, H., 1984, "Theoretical Study of Fluid Forces on Whirling Centrifugal Impeller," in Japanese, *Trans. JSME*, Vol. 50, No. 458, B, pp. 2518-2523, also 1987, "Lateral Fluid Forces on Whirling Centrifugal Impeller (1st Report: Theory)" *ASME Journal of Fluids Engineering*, Vol. 109, No. 2, pp. 94-99.
 Thompson, W. E., 1978, "Fluid Dynamic Excitation of Centrifugal Compressor Rotor Vibrations," *ASME Journal of Fluids Engineering*, Vol. 100, No. 1, pp. 73-78.
 Tsujimoto, Y., Imaichi, K., Tomohiro, T., and Gotou, M., 1986, "A Two-Dimensional Analysis of Unsteady Torque on Mixed Flow Impellers," *ASME Journal of Fluids Engineering*, Vol. 108, No. 1, pp. 26-33.

Derivation of Basic Equations

Derivation of Equation (1)

Let us start from equation (3), page 80 of Milne-Thomson (1968):

$$\frac{\partial \mathbf{v}}{\partial t} - \mathbf{v} \times (\nabla \times \mathbf{v}) + \nabla \left(\frac{p}{\rho} + \frac{1}{2} \mathbf{v}^2 \right) = \mathbf{f}$$

where a body force \mathbf{f} is added. Consider a frame whose origin is translating with a velocity \mathbf{U} and rotating with an angular velocity Ω . We represent the absolute velocity by \mathbf{v} , the velocity relative to the moving frame \mathbf{w} , and the velocity of a point fixed to the moving frame $\mathbf{V} = \mathbf{v} - \mathbf{w} = \mathbf{U} + \Omega \times \mathbf{x}'$ where \mathbf{x}' is the position vector in the moving frame. $\partial/\partial t'$ means the time derivative at a point fixed to the moving frame. Unit vectors in the stationary and moving frame are represented by \mathbf{e}_i and \mathbf{e}'_i , respectively, and the components of \mathbf{v} in these directions v_i and v'_i . Now we have

$$\frac{\partial \mathbf{v}}{\partial t'} \equiv \frac{\partial}{\partial t'} (v_i \mathbf{e}_i) = \frac{\partial v_i}{\partial t'} \mathbf{e}_i = \frac{\partial \mathbf{v}}{\partial t} + (\mathbf{V} \cdot \nabla) \mathbf{v}$$

and

$$\begin{aligned} \frac{\partial \mathbf{v}}{\partial t'} &= \frac{\partial}{\partial t'} (v_i \mathbf{e}_i) = \frac{\partial}{\partial t'} (v'_i \mathbf{e}'_i) = \frac{\partial v'_i}{\partial t'} \mathbf{e}'_i \\ &+ v'_i \frac{\partial \mathbf{e}'_i}{\partial t'} = \frac{\partial \mathbf{v}}{\partial t^*} + \Omega \times \mathbf{v} \end{aligned}$$

where we have defined

$$\frac{\partial \mathbf{v}}{\partial t^*} \equiv \frac{\partial v'_i}{\partial t'} \mathbf{e}'_i$$

From the above two equations we obtain

$$\frac{\partial \mathbf{v}}{\partial t} = \frac{\partial \mathbf{v}}{\partial t^*} + \Omega \times \mathbf{v} - (\mathbf{V} \cdot \nabla) \mathbf{v}$$

Using this equation and identities

$$\frac{1}{2} \mathbf{v}^2 = \frac{1}{2} \mathbf{w}^2 - \frac{1}{2} \mathbf{V}^2 + \mathbf{v} \cdot \mathbf{V},$$

$$\nabla (\mathbf{v} \cdot \mathbf{V}) = -\Omega \times \mathbf{v} + \mathbf{V} \times (\nabla \times \mathbf{v}) + (\mathbf{V} \cdot \nabla) \mathbf{v}$$

we obtain equation (1) in the main text.

Derivation of Equation (2)

Since $\partial \mathbf{v}/\partial t^*$ in equation (1) is represented by the components in the moving frame we can easily take out the component of equation (1) in the direction of the vane surface. In an actuator impeller, \mathbf{w} is parallel to the vane surface and hence the third term is normal to it. In case of inviscid flow, the body force \mathbf{f} , which represents the force exerted by the vanes of the actuator impeller, is normal to the vane surface. Hence the component of equation (1) parallel to the vane surface can be written as

$$\frac{\partial v_s}{\partial t^*} + \frac{\partial}{\partial s} \left\{ \frac{1}{2} \mathbf{w}^2 - \frac{1}{2} (\mathbf{U} - \Omega \times \mathbf{x}')^2 + \frac{p}{\rho} \right\} = 0$$

where s represents a coordinate along a vane surface or a component in its direction. By integrating this equation we can easily obtain the pressure difference between the inlet and outlet of a flow passage. Using this pressure difference and representing the velocity in terms of those relative to the z' frame we obtain the difference of the total pressure $p_t \equiv p + (\rho/2)v^2$, where v is the absolute velocity, given by equation (2).